Supplementary Information

Layer-coupled corner states in two-dimensional topological multiferroics

Runhan Li,[1] Xiaorong Zou,[1] Yingxi Bai,[1] Zhiqi Chen,[1] Baibiao Huang,[1] Ying Dai,[1, *] and Chengwang Niu[1, *]

[1]School of Physics, State Key Laboratory of Crystal Materials, Shandong University, Jinan 250100, China

S1 Detailed analysis for the tight-binding Hamiltonian

Here, a symmetry constrained tight-binding (TB) bilayer model has been constructed based on the $d_{z^2}, d_{xy}, d_{x^2-y^2}$ orbitals. This TB model for the magnetic bilayer can be expressed as follows:

$$\begin{aligned} H_0 &= H^A + H^B + H^{AB} + H_{os}, \\ H^{\eta} &= \sum_{\langle i,j\rangle} \sum_{n,n',\sigma} t_{nn'} c^{\dagger}_{\eta n\sigma}(r_i) c_{\eta n'\sigma}(r_j), \\ H^{AB} &= \sum_{\langle i,j\rangle} \sum_{n,n',\sigma} t'_{nn'} c^{\dagger}_{An\sigma}(r_i) c_{Bn'\sigma}(r_j) + h.c., \\ H_{os} &= \sum_{i,\eta,n,\sigma} \Delta_n c^{\dagger}_{\eta n\sigma}(r_i) c_{\eta n\sigma}(r_i). \end{aligned}$$

Here, the Hamiltonian H_0 includes intra-layer nearest-neighbor (NN) hopping contributions H^A and H^B, inter-layer NN hopping term H^{AB} and the last term H_{os} describes the on-site energy. $c^{\dagger}_{\eta n\sigma}(r_i)$ ($c^{\dagger}_{\eta n'\sigma}(r_j)$) represents the creation (annihilation) operator for an electron with spin σ on site i (site j), where n, n' denotes different orbitals and $\eta = A, B$ represents different sublattices corresponding to the upper and lower layers of the model. $t_{nn'}$, $t'_{nn'}$, and Δ_n denote intralayer NN hopping, interlayer NN hopping, and on-site energy strength, respectively. Under the constraint of D_{3h} point group symmetry, the intra-layer hopping terms are reduced to six parameters, while the inter-layer hopping terms are reduced to two parameters while preserving spin degeneracy. The Hamiltonian $H_0(k)$ in the momentum space representation under the constraint of symmetry operation *R* can be written as

$$P(R)^{-1} H(\boldsymbol{k}) P(R) = H(\hat{R}^{-1}\boldsymbol{k}).$$

The point group D_{3h} contains the discrete rotation symmetry C_3 (axis is perpendicular to the plane), mirror symmetry M_z, mirror symmetry M_x, and any of their combination. Considering symmetry restrictions on the model hopping parameters, we start from the three-band nearest-neighbor hopping TB model for the TMDs monolayer, and the Hamiltonian can be expressed as [1]

$$H_0(\mathbf{k}) = \begin{bmatrix} h_{11} & h_{12} & h_{13} & h_1^{'} & & \\ h_{12}^{*} & h_{22} & h_{23} & & h_2^{'} & \\ h_{13}^{*} & h_{23}^{*} & h_{33} & & & h_2^{'} \\ h_1^{'} & & & h_{11} & h_{12} & h_{13} \\ & h_2^{'} & & h_{12}^{*} & h_{22} & h_{23} \\ & & h_2^{'} & h_{13}^{*} & h_{23}^{*} & h_{33} \end{bmatrix},$$

where

$$h_{11} = 2t_1(\cos 2\alpha + 2\cos\alpha\cos\beta) + \epsilon_1,$$

$$h_{12} = -2\sqrt{3}t_3\sin\alpha\sin\beta + 2it_2(\sin 2\alpha + \sin\alpha\cos\beta),$$

$$h_{13} = 2t_3(\cos 2\alpha - \cos\alpha\cos\beta) + 2\sqrt{3}it_2\cos\alpha\sin\beta,$$

$$h_{22} = 2t_4\cos 2\alpha + (t_4 + 3t_6)\cos\alpha\cos\beta + \epsilon_2,$$

$$h_{23} = \sqrt{3}(t_6 - t_4)\sin\alpha\sin\beta + 4it_5\sin\alpha(\cos\alpha - \cos\beta),$$

$$h_{33} = 2t_6\cos 2\alpha + (3t_4 + t_6)\cos\alpha\cos\beta + \epsilon_2,$$

$$h_1^{'} = t_1^{'},$$

$$h_2^{'} = t_2^{'},$$

$$(\alpha, \beta) = (\frac{1}{2}k_x a, \frac{\sqrt{3}}{2}k_y a).$$

Subsequently, we further consider the interaction of spin-orbit coupling (SOC) by the on-site contribution term $\boldsymbol{L}\cdot\boldsymbol{S}$ and magnetic field interactions, and add the two term to the model as:

$$H = H_0 + H_{SOC} + H_M .$$

In which

$$H_{SOC} = t_{so}\boldsymbol{L}\cdot\boldsymbol{S},$$

$$H_M = t_m\boldsymbol{B}\cdot\boldsymbol{S},$$

where t_{so} denotes the on-site SOC strength, and $\boldsymbol{B}=(0,0,\boldsymbol{B}_z)$ represents the directions of magnetic field with a strength of t_m. t_{so}=0.5 eV and t_m=3.0 eV are used. Where H_{SOC} and H_M are on-site SOC interaction with strength t_{so} and exchange field (magnetic field) terms with strength t_m, respectively. $\boldsymbol{B}=(\boldsymbol{B}_x,\boldsymbol{B}_y,\boldsymbol{B}_z)$ represents the directions of the magnetic field. To investigate systems with broken M_z symmetry, we introduce a new parameter, denoted as $e^{\pm\gamma}$, by replacing H^A with $e^{\gamma}H^A$ and H^B with $e^{-\gamma}H^B$ in the Hamiltonian H.

Table S1. The parameters amplitudes in eV of the d-orbitals TB bilayer model with SOC and exchange field terms.

hopping	ϵ_1	ϵ_2	t_1	t_2	t_3	t_1'
	t_4	t_5	t_6	t_{so}	t_m	t_2'
strength	1.746	2.804	−0.184	0.401	0.507	2.0
	0.02	0.338	0.057	0.5	3.0	2.0

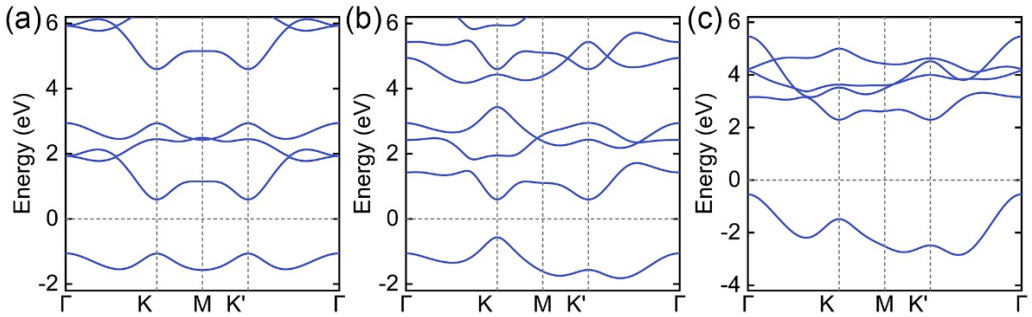

Figure S1. The band structures of TB model with (a) t_{so} = 0.0 eV, t_m = 0.0 eV, γ = 0.0; (b) t_{so} = 0.5 eV, t_m = 3.0 eV, γ = 0.0; and (c) t_{so} = 0.5 eV, t_m = 3.0 eV, γ = 1.0.

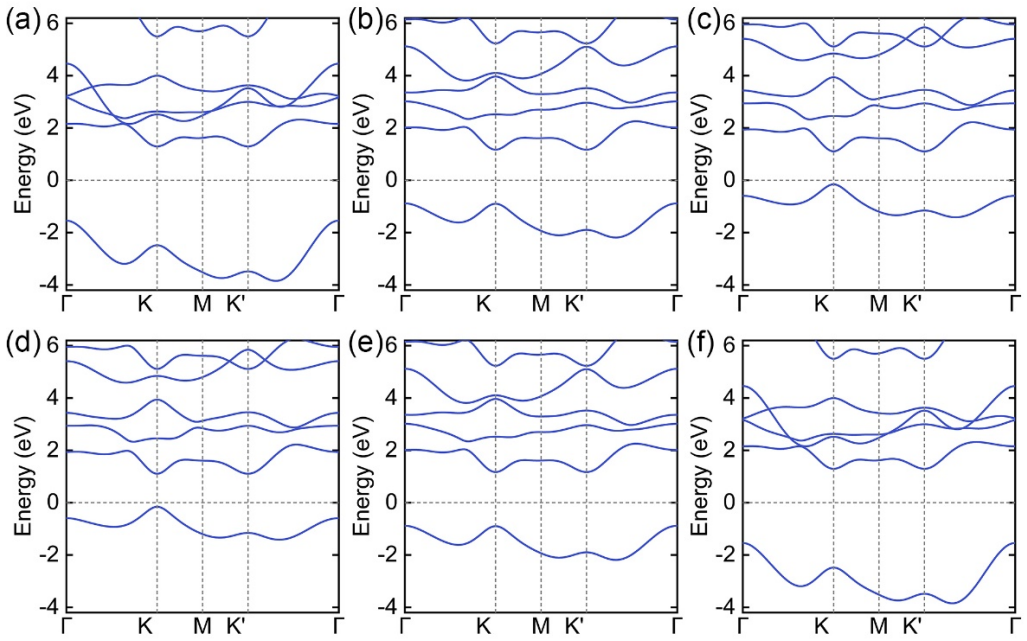

Figure S2. The band structures of TB model with (a) γ = -1.0 eV, (b) γ = -0.6 eV, (c) γ = -0.2 eV, (d) γ = 0.2 eV, (e) γ = 0.6 eV, and (f) γ = 1.0 eV. Throughout this range, as the initial polarization state evolves to the final polarization state of the TB model, the band gap remains unclosed, suggesting the same topological phase.

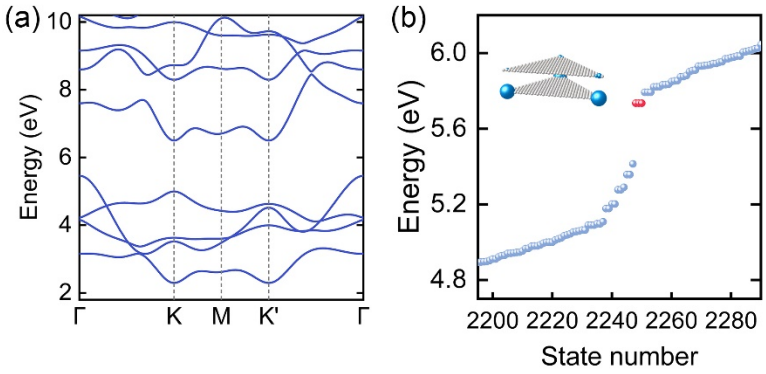

Figure S3. (a) Band structure of the TB model with 5 occupied bands. (b) Energy spectrum of a triangular nanoflake for the TB model, where the nontrivial corner states are marked by red dots. Inset shows perspective views of the total charge distribution of the corresponding corner states.

S2 Computational method

First-principles calculations were conducted within the framework of density functional theory (DFT) employing the projector augmented wave (PAW) method as implemented in the Vienna ab initio simulation package (VASP) [2, 3]. The Perdew-

Burke-Ernzerhof (PBE) formulation of the generalized gradient approximation (GGA) was employed for the exchange-correlation potential [4]. A cutoff energy of 600 eV was utilized, and structural relaxation was performed until the residual forces were below 0.01 eV/Å. To prevent interactions between adjacent slabs, a vacuum layer of 20 Å was introduced. We systematically calculated the band structure and topological states of the material for various U values for the Co-d electrons (ranging from 1.5 to 3.5 eV). The results indicate that the band structure near the Fermi level is insensitive to changes in U values, with only slight modifications in the band gap. Variations in U values do not influence the second-order topological phase of the material. In the main text, we employed the results obtained with U = 2 eV for analysis. Phonon calculations, based on density functional perturbation theory, were carried out using the PHONOPY package. The construction of maximally localized Wannier functions (MLWFs) was constructed in the basis of C/N-p, F-p and Co-d by using the WANNIER90 code [5], which combined the results of first-principles calculations from VASP.

S3 Detailed analysis for Monte Carlo simulations

The ferromagnetic Curie temperature T_c of H'-Co_2CF_2 is evaluated by the method of Monte Carlo (MC) simulations. Based on the Heisenberg model, the spin Hamiltonian can be expressed as

$$\hat{H} = -\sum_{\langle ij \rangle} J_1 \overrightarrow{S_i} \cdot \overrightarrow{S_j} - \sum_{\langle\langle ij \rangle\rangle} J_2 \overrightarrow{S_i} \cdot \overrightarrow{S_j} - \sum_{<i>} A\left(S_i^z\right)^2,$$

where $\overrightarrow{S_i}$ is the spin vector on the atomic site *i*, J_1 and J_2 are the nearest neighboring (NN) and next NN isotropic exchange interaction parameters, respectively. We assumed that the A comes solely from the MCA term to get a finite value of T_c. As shown in Fig. S4, the parameters J_1 and J_2 were calculated by the energy mapping analysis of FM, AFM-1 and AFM-3 spin configurations,

$$E_{FM-z} = E_0 - 3J_1S^2 - 3J_2S^2 - AS^2,$$
$$E_{AFM1} = E_0 + J_1S^2 + J_2S^2 - AS^2,$$
$$E_{AFM3} = E_0 - J_1S^2 + J_2S^2 - AS^2,$$

with the normalized magnetization of |S| = 1. J_1 and J_2 are calculated to be 51.7 meV, 4.3 meV, respectively. Fig. S5 shows the evolution of normalized magnetic moment as a function of temperature, indicating that Tc = 740 K for H'-Co_2CF_2. The value is much

larger than the previously reported 2D ferromagnetic CrI_3 (45K).

Using the Berry phase approach, our first-principles calculations predict a spontaneous electric polarization of approximately $0.2\times10^{-10}\,\mathrm{C/m}$ for H'-Co_2CF_2. To estimate the ferroelectric Curie temperature, we used the Landau theory with the polarization P as the order parameter. The system free energy is expressed in the Landau-Ginzburg-type expansion [6-8]:

$$F=\sum_i\left(\frac{A}{2}P_i^2+\frac{B}{4}P_i^4+\frac{C}{6}P_i^6\right)+\frac{D}{2}\sum_{\langle i,j\rangle}\left(P_i-P_j\right)^2 \quad (1)$$

where P_i is the polarization of each unit cell. The first three terms are associated with the energy contribution from the local modes up to the sixth order. The parameter D is determined through the mean-field approximation. The fitted parameters are given in Table S2. Monte Carlo simulations were performed with the effective Hamiltonian in Eq. (1), resulting in a ferroelectric Curie temperature of 720 K, as shown in Fig. S6 (a). At the same time, we calculated the ferroelectric Curie temperature of GeTe using the same method, adopting parameters from a previous publication [8]. As shown in Fig. S6 (b), it is found to be around 570 K, consistent with previous reports.

Table S2. The spontaneous polarization P (10^{-10} C/m) at zero temperature, the fitted parameters A, B, C, and D in Eq. (1), and the estimated ferroelectric Curie temperature T_C (K).

Material	P	$A(\times 10^2)$	$B(\times 10^4)$	$C(\times 10^6)$	$D(\times 10^2)$	T_C
H '-Co_2CF_2	0.2	-118.048	23.187	0.084	7.940	720

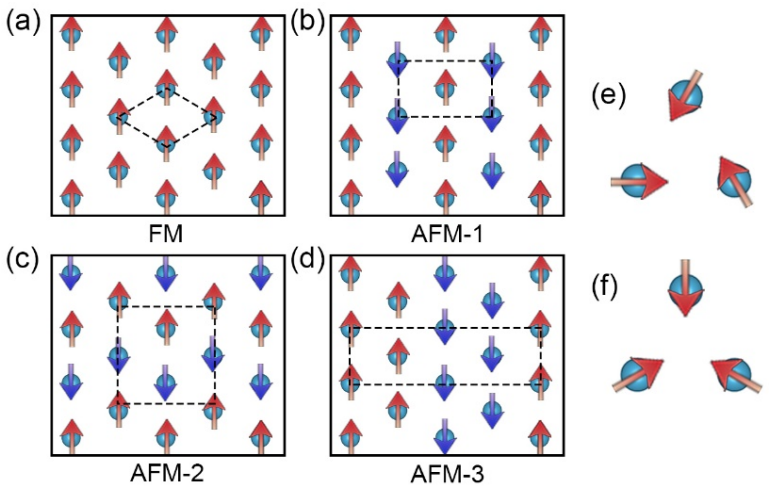

Figure S4. Sketch of six considered magnetic configurations: (a) FM, (b) AFM-1, (c) AFM-2, (d) AFM-3, (e) frustrated AFM-1 and (f) frustrated AFM-2.

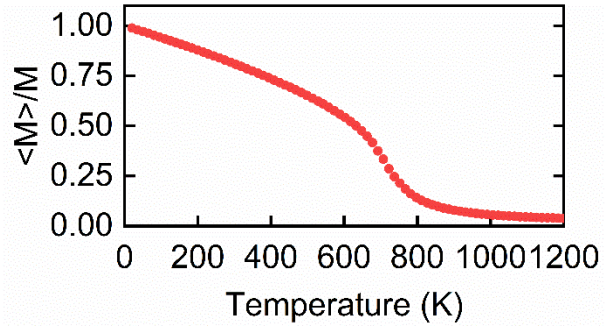

Figure S5. Normalized magnetic moments as a function of temperature by MC simulations for H '-Co_2CF_2.

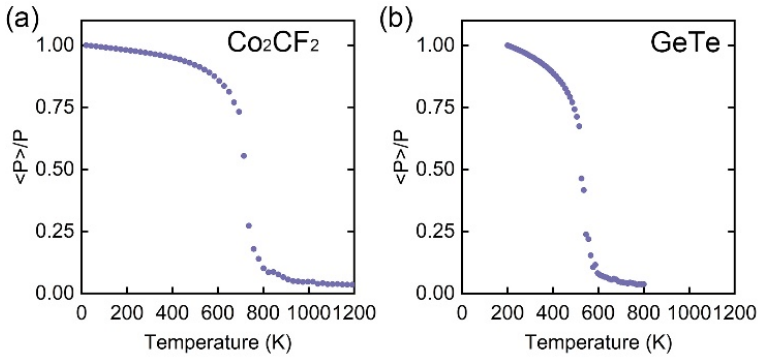

Figure S6. Normalized polarization as a function of temperature by MC simulations for (a) H'-Co_2CF_2 and (b) GeTe. The ferroelectric Curie temperatures for H'-Co_2CF_2 and GeTe are estimated to be of 720 and 570 K, respectively. The result of GeTe is consistent with previous reports.

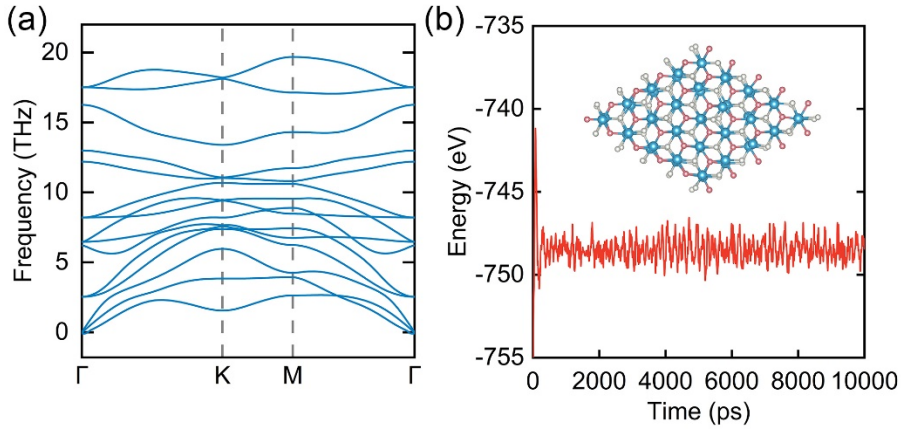

Figure S7. (a) The calculated phonon dispersion and (b) ab initio molecular dynamics simulation results of H'-Co_2CF_2. Insert in (b) is snapshot of the structure for H'-Co_2CF_2 taken from the end of ab initio molecular dynamics simulation (500 K and 10 ps).

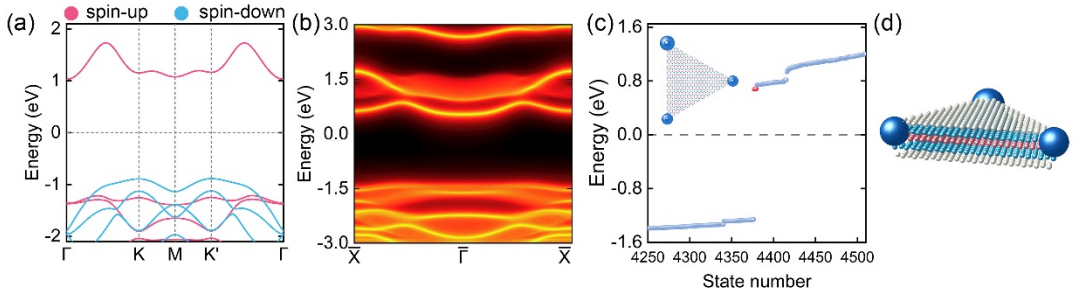

Figure S8. (a) Spin-resolved band structure of the ferroelectric Co_2CF_2 with out-of-plane ferromagnetic configuration using HSE method. (b) The corresponding topological edge spectrum for the spin-up channel. (c, d) Energy spectrum and charge distributions of triangular nanoflakes of H'-Co_2CF_2 for the spin-up channel, where the nontrivial corner states are marked by red dots.

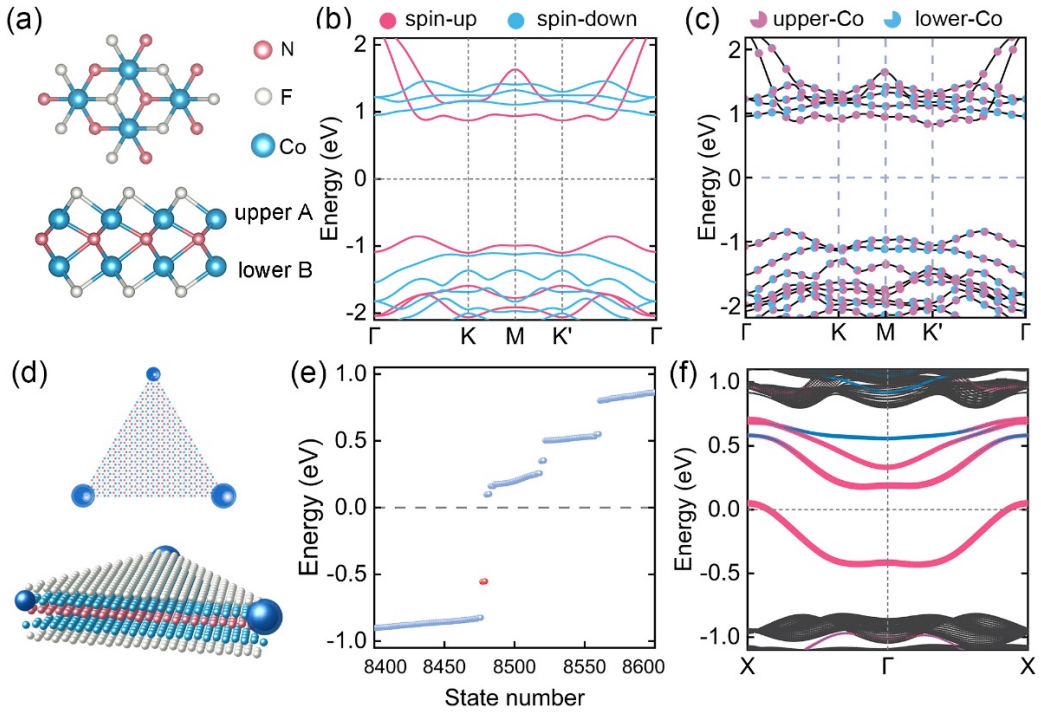

Figure S9. (a) Top and side views of the ferroelectric H'-Co_2NF_2 under upward polarization. (b) Spin-resolved band structures under upward polarization without SOC. Red and blue lines represent the spin-up and spin-down states, respectively. (c) Layer-resolved band structure under with SOC. The scatters, symbolized by small pie charts, represent weighted distributions with red and blue indicating the upper- and lower-Co layers. (e) The energy spectrum of the ferroelectric H'-Co_2NF_2 under upward polarization, and (d) show the total charge distribution of three occupied corner states. (f) Band structures for a nanoribbon in the x direction and infinite along the y direction for H'-Co_2NF_2 under upward polarization.

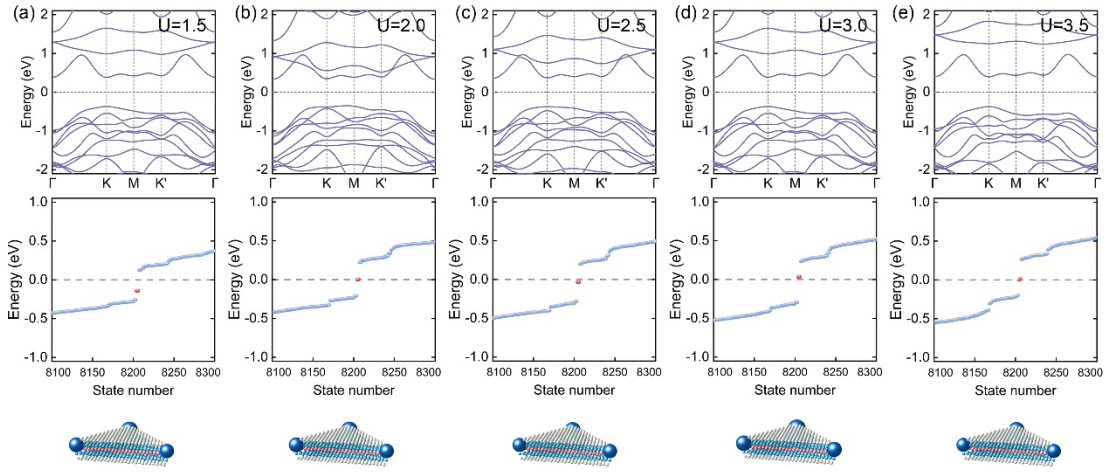

Figure S10. Band structures and energy spectra and charge distributions of H'-Co_2CF_2 with out-of-plane ferromagnetic configuration under (a) U =1.5 eV, (b) 2.0 eV, (c) 2.5 eV, (d) 3.0 eV, and (e) 3.5 eV. The results indicate that the topological corner states are robust against the values of U.

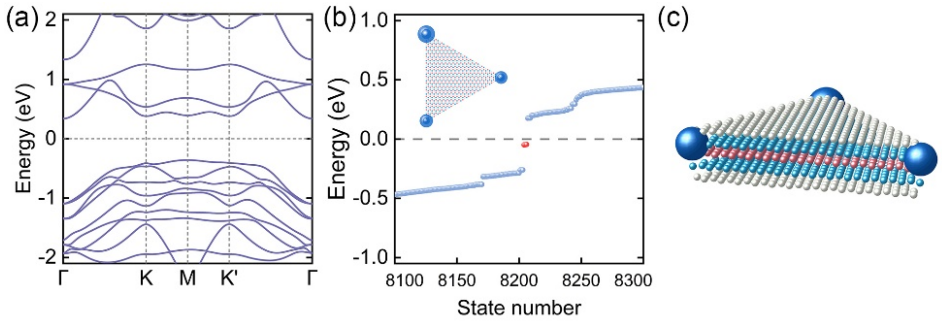

Figure S11. (a) The band structure of H'-Co_2CF_2 with in-plane ferromagnetic configuration. (b, c) Energy spectrum and charge distributions of triangular nanoflakes of H'-Co_2CF_2 with in-plane ferromagnetic configuration, where the nontrivial corner states are marked by red dots. With an in-plane magnetic orientation, similar topological properties are obtained as with out-of-plane magnetization, demonstrating that H'-Co_2CF_2 is a robust SOTI regardless of the magnetization directions.

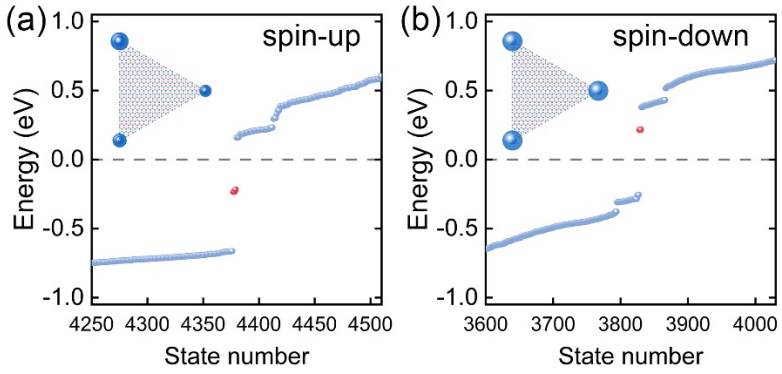

Figure S12. Energy spectra of triangular nanoflakes of H'-Co_2CF_2 for (a) the spin-up channel and (b) the spin-down channel, where the occupied corner states are marked by red dots. Insets show the total charge distribution of the three occupied corner states. The second-order topological phases are obtained for both spin channels.

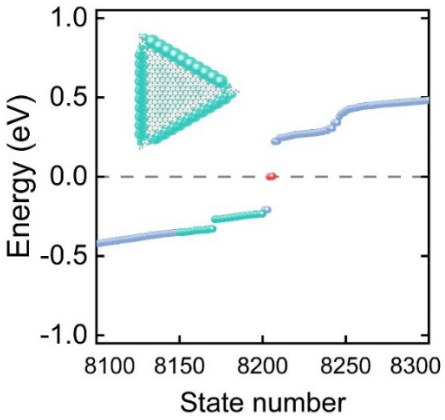

Figure S13. Energy spectrum of a triangular nanoflake for H'-Co_2CF_2 with SOC, where the trivial states are marked by green dots. Inset shows the total charge distribution of these trivial states, with electrons primarily distributed along the edges and interior of the nanoflake.

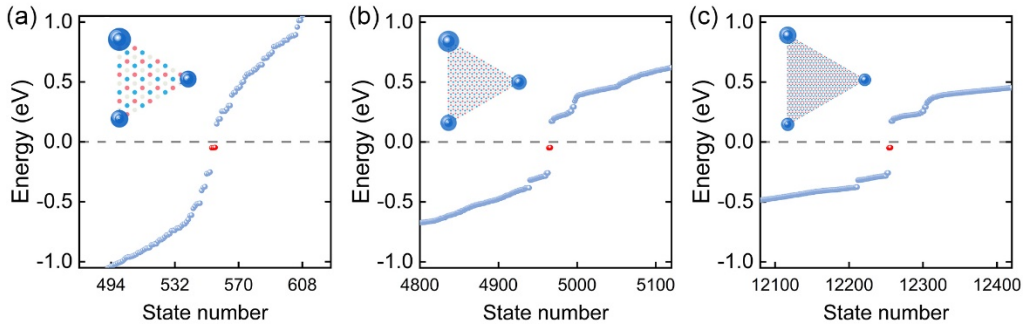

Figure S14. Energy spectrums of triangular nanoflakes of H'-Co_2CF_2 with (a) 15 Å, (b) 50 Å, (c) 79 Å with out-of-plane ferromagnetic configuration. Insets show the total charge distribution of the three occupied corner states.

References

[1] Liu, G.-B.; Shan, W.-Y.; Yao, Y.; Yao, W.; Xiao, D. Phys. Rev. B 88, 085433 (2013).

[2] G. Kresse and J. Hafner, Phys. Rev. B 47, 558 (1993).

[3] G. Kresse and J. Furthmüller, Phys. Rev. B 54, 11169 (1996).

[4] J. P. Perdew, K. Burke, and M. Ernzerhof, Phys. Rev. Lett. 77, 3865 (1996).

[5] A. A. Mostofi, J. R. Yates, Y.-S. Lee, I. Souza, D. Vanderbilt, and N. Marzari, Comput. Phys. Commun. 178, 685 (2008).

[6] R. Cowley, Adv. Phys., 29, 1 (1980).

[7] R. Fei, W. Kang and L. Yang, Phys. Rev. Lett., 117, 097601 (2016).

[8] W. Wan, C. Liu, W. Xiao and Y. Yao, Appl. Phys. Lett., 111, 132904 (2017).